# Quadrupolar NMR Spin Relaxation Calculated Using Ab Initio Molecular Dynamics: Group 1 and Group 17 Ions in Aqueous Solution

Shyam Badu,[†] Lionel Truflandier,[‡] and Jochen Autschbach*,[†]

[†]Department of Chemistry, University at Buffalo—State University of New York, Buffalo, New York 14260-3000, United States
[‡]Institut des Sciences Moléculaires, Université Bordeaux I, 351 Cours de la Libration, 33405 Talence, France

ABSTRACT: Electric field gradient (EFG) fluctuations for the monoatomic ions $^7Li^+$, $^{23}Na^+$, $^{35}Cl^-$, $^{81}Br^-$, and $^{127}I^-$ in aqueous solution are studied using Car–Parrinello ab initio molecular dynamics (aiMD) simulations based on density functional theory. EFG calculations are typically performed with 1024 ion–solvent configurations from the aiMD simulation, using the Zeroth Order Regular Approximation (ZORA) relativistic Hamiltonian. Autocorrelation functions for the spherical EFG tensor elements are computed, transformed into the corresponding spectral densities (under the extreme narrowing condition), and subsequently converted into NMR quadrupolar relaxation rates for the ions. The relaxation rates are compared with experimental data. The order of magnitude is correctly predicted by the simulations. The computational protocol is tested in detail for $^{81}Br^-$.
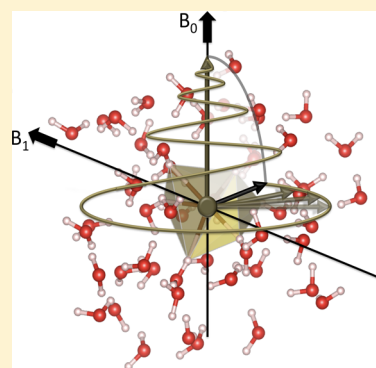
1. INTRODUCTION

Solution-state and solid-state NMR experiments often focus on chemical shifts, dipolar and J-coupling, quadrupolar coupling, and the tensor properties of these observables. However, the nuclear spin relaxation rates also contain a wealth of information about structure and dynamics of a system. For nuclei with spin $S \geq 1$, relaxation via quadrupolar interactions is usually thought to be the dominant effect.[1] Other relaxation mechanisms that affect all types of spins are facilitated by dipolar and J-coupling, chemical shift anisotropy (CSA), chemical exchange, and, for paramagnetic systems, electron-spin nuclear-spin interactions.[1] For an application of classical molecular dynamics to the CSA-driven nuclear spin relaxation of ^{129}Xe, see ref 2. An example for a paramagnetic system, Gd^{3+} in aqueous solution modeled by classical molecular dynamics, can be found in ref 3. We focus herein on diamagnetic species and quadrupolar relaxation in solution.

Quantum mechanics (QM)-based ab initio molecular dynamics (aiMD) simulations, coupled to QM calculations of NMR parameters, have been of great utility in predicting dynamic medium effects and the effects of nuclear vibrations on NMR chemical shifts and J-couplings in solution (see, for instance, refs 4–8). With aiMD, it is further possible to investigate relaxation phenomena microscopically in great detail without recourse to semiempirical methods such as molecular force fields or model potentials. From a single or a set of computed aiMD trajectories, the relaxation times T_1 and T_2 (or relaxation rates $R_1 = 1/T_1$, $R_2 = 1/T_2$) of an NMR active nucleus can be determined using the relaxation theories of Bloembergen, Solomon, and Redfield.[9–11] In aiMD, the nuclei are typically treated as classical particles but the forces driving the dynamics are obtained from a QM treatment of the electrons. A nuclear quadrupole moment interacts with the electric field gradient (EFG) caused by surrounding charge distributions. A quantum mechanical treatment of the electrons gives access to the intramolecular mechanisms responsible for the electronic component of the EFG at a nucleus, along with the EFG caused by electron charge distributions of neighboring and distant molecules. Together with the nuclear contributions to the EFG, this information allows one to determine the tensor parameters for the quadrupolar interactions, and, ultimately, the relaxation rates.

The present work is concerned with relaxation rates for a set of Group 1 cations ($^7Li^+$, $^{23}Na^+$) and Group 17 anions ($^{35}Cl^-$, $^{81}Br^-$, $^{127}I^-$) in aqueous solution. These systems are well-characterized,[12,13] which renders them ideal for an application of aiMD-based relaxation rate calculations. Experimental data are available in the literature.[14] The relaxation rates exhibit systematic trends as a function of ion type, concentration, and the viscosity of the solution.[15–19] Group 1 ions (in particular, $^{23}Na^+$) are interesting for several reasons. For instance, T_1 and T_2 measurements of $^{23}Na^+$ in biological tissue have found sound medical applications. $^{23}Na^+$ relaxation time measurements were shown to be useful to investigate cartilage damage in vivo.[20,21] T_2 measurements of $^{23}Na^+$ have also been used in a pioneering study of spinal disk degeneration.[22]

Calculations of quadrupolar relaxation rates of ions in solution are also highly interesting on a fundamental level. The isolated ions have spherical charge distributions, and, therefore,

the EFG at the nucleus vanishes. An instantaneous EFG is induced by fluctuations in the surrounding of the ion, via electrostatic polarization of the ion or by contact with solvent molecules (orbital interactions), and via a fluctuating non-spherical distribution of partial charges of solvent molecules. The latter effect is potentially amenable to a treatment by simple point charges. However, even for distant solvent molecules, there are caveats. For example, for the solvent water, the partial charges for oxygen and hydrogen in the water molecules in the liquid must be carefully calibrated to reflect the water dipole moment in solution (which is very different from the gas phase[23]). Point-charge models such as the TIP family[24] have been developed in order to reproduce the structure of liquid water. These, or QM embedding methods,[23] may be suitable to treat distant waters in relaxation rate calculations. For closer contacts between solute and solvent, as well as between solvents near the solute, minute details of changes in the electronic structure of both species upon their interactions likely require an explicit QM treatment. Recent work reported an application of a combination of QM with a polarizable force field for the solvent to calculate the EFG of $^{23}Na^+$ in solution, based on classical MD simulations.[25] The importance of a QM treatment of the ion has been highlighted, calling into question the applicability of the Sternheimer approximation[26] used to treat the ion polarization. aiMD has been shown to correctly describe the liquid structure of water.[27] Furthermore, proton and ^{17}O quadrupolar relaxation rates in liquid water have been calculated by aiMD.[28] The study reported agreement with experimental relaxation rates as far as the order of magnitude is concerned, and it was demonstrated that the behavior of the EFG autocorrelation functions may be very different from a simple monoexponential decay.

We have recently started to developed a module for the Quantum-Espresso (QE) suite of programs,[29] with the objective of treating a variety of nuclear spin-relaxation mechanisms based on aiMD simulations. Recent aiMD studies performed within our group[30−32] have necessitated the implementation of a module called "DynPro" (dynamic properties) in QE to facilitate the analysis of aiMD trajectories, create solute−solvent clusters for external NMR programs, and compute nuclear velocity autocorrelation functions to generate vibrational spectra. An extension of DynPro has been developed for the present study which implements quadrupolar relaxation rate calculations. The EFG tensors entering the computation can be obtained, in principle, directly from the periodic plane-wave DFT code (which is suitable for light nuclei at the nonrelativistic nonhybrid DFT level), or from an external molecular QM package by constructing suitable solute−solvent clusters for configurations along the aiMD trajectory. We chose the latter approach, since it allows for relaxation studies across the periodic table by using relativistic molecular electronic structure methods, along with a large variety of density and hybrid density functionals.

This paper is organized as follows. In section 2, we describe the formalism used for the calculations, and some details of the implementation. Section 3 outlines the computational procedure. The results are presented and discussed in section 4, which is divided into two parts. First, a suitable computational protocol for quadrupolar relaxation is developed, using $^{81}Br^-$ as a test case. The remainder of section 4 is devoted to a comparison of computed results with experiment. Concluding remarks and an outlook can be found in section 5.

2. THEORY

This section provides a synopsis of the formalism used to calculate the quadrupolar relaxation rates. Additional details about the formalism can be found in ref 26 and refs 33−36. It is important to consider the tensor nature of the nuclear quadrupolar interactions.[37−39] From a multipole expansion, the Hamiltonian describing the quadrupolar interaction of a nucleus with a spin $>^1/_2$ with a surrounding charge distribution can be expressed as

$$H_Q = \sum_{\alpha,\beta} \left(\frac{\partial^2 V}{\partial r_\alpha \partial r_\beta} \right)_0 Q_{\alpha\beta} \tag{1}$$

In eq 1, the indices α and β indicate one of the Cartesian coordinates, x, y, or z. Furthermore, V is the potential energy of the nucleus interacting with surrounding charges, and the subscript "0" indicates that the derivatives are taken at the position of the nucleus. Let $\mathcal{E}_\alpha$ be a component of the electric field. The electric field gradient (EFG) then can be defined as

$$V_{\alpha\beta} = \frac{\partial^2 V}{\partial r_\alpha \partial r_\beta} = -\frac{\partial \mathcal{E}_\alpha}{\partial r_\beta} = -\frac{\partial \mathcal{E}_\beta}{\partial r_\alpha} \tag{2}$$

The $Q_{\alpha\beta}$ in eq 1 are tensor operators defining the characteristic features of the quadrupolar interaction and can be expressed as

$$Q_{\alpha\beta} = \frac{eQ}{6I(2I-1)} \left[\frac{3}{2}(I_\alpha I_\beta + I_\beta I_\alpha) - \delta_{\alpha\beta} I(I+1) \right] \tag{3}$$

with Q being the nuclear quadrupole moment, e the unit charge, I_α a component of the nuclear spin vector operator $\mathbf{I}$, and I the spin quantum number. Alternatively, the quadrupole interaction can be expressed in terms of spherical tensor operators $\Gamma_{l,m}$ of rank $l = 2$,

$$H_Q = \sum_{m=-2}^{2} \Gamma_{2,m} \tag{4}$$

where

$$\Gamma_{2,m} = \frac{eQ}{2I(2I-1)}(-1)^m T_{2,m} R_{2,-m} \tag{5}$$

The set of $T_{2,m}$, for a single spin, are given by

$$T_{2,0} = \frac{1}{\sqrt{6}}[3I_z^2 - I(I+1)] \tag{6a}$$

$$T_{2,\pm 1} = \sqrt{\frac{1}{2}}(I_z I_\pm + I_\pm I_z) \tag{6b}$$

$$T_{2,\pm 2} = I_\pm I_\pm \tag{6c}$$

with the spin ladder operators

$$I_\pm = \mp \sqrt{\frac{1}{2}}(I_x \pm iI_y) \tag{7}$$

The spatial components $R_{2,m}$ are calculated from the Cartesian components of the EFG tensor as[40]

$$R_{2,0} = 3\sqrt{\frac{1}{6}} V_{zz} \tag{8a}$$

$$R_{2,\pm 1} = \mp V_{xz} - iV_{yz} \tag{8b}$$

$$R_{2,\pm 2} = \frac{1}{2}(V_{xx} - V_{yy}) \pm iV_{xy} \tag{8c}$$

The V matrix can be diagonalized, such that the EFG tensor is given in terms of three principal components—V_{11}, V_{22}, and V_{33}—and the orientation of the principal axis system (PAS), relative to the laboratory coordinates or some other reference frame. In ref 39, expressions similar to eqs 1 and 4 have been given specifically for the PAS system of the EFG tensor. By convention, the principal component ordering is such that

$$|V_{33}| \geq |V_{22}| \geq |V_{11}| \tag{9}$$

The EFG tensor is traceless,

$$\sum_i V_{ii} = 0 \tag{10}$$

leaving only two independent parameters. The tensor asymmetry parameter is given by

$$\eta_Q = \frac{V_{11} - V_{22}}{V_{33}} \tag{11}$$

from which follows

$$V_{11} = -\frac{1}{2}(1 + \eta_Q)V_{33} \tag{12}$$

$$V_{22} = -\frac{1}{2}(1 - \eta_Q)V_{33} \tag{13}$$

In other words, the EFG tensor is fully characterized by V_{33}, η_Q, and the orientation of the PAS. In solid-state NMR experiments, the magnitude of the EFG manifests itself as the magnitude of the nuclear quadrupole coupling constant.

$$C_Q = \frac{1}{h}eQV_{33} \tag{14}$$

A factor of $0.2350Q$ MHz/mbarn converts the EFG from atomic units to a quadrupole coupling constant in MHz, with Q in units of mbarn (10^{-31} m^2). A collection of updated nuclear quadrupole moments can be found in ref 41.

We follow the formalism as presented by Spiess[35] and by Cowan[36] to gain access to the quadrupolar relaxation rates. The longitudinal and transverse relaxation rates, $1/T_1$ and $1/T_2$, can be expressed as

$$\frac{1}{T_1} = \frac{e^2 Q^2 (2I + 3)}{40 I^2 (2I - 1)\hbar^2}[G_{2,0}^Q] \tag{15a}$$

$$\frac{1}{T_2} = \frac{e^2 Q^2 (2I + 3)}{40 I^2 (2I - 1)\hbar^2}[G_{2,\pm 1}^Q] \tag{15b}$$

In eq 15b, either $G_{2,1}^Q$ or $G_{2,-1}^Q$ can be used to calculate the result. The quantities $G_{2,0}^Q$ and $G_{2,\pm}^Q$ are defined as

$$G_{2,0}^Q = 4g_{2,2}^Q(2\omega_0) + g_{2,1}^Q(\omega_0) + g_{2,-1}^Q(-\omega_0)$$
$$+ 4g_{2,-2}^Q(-2\omega_0) \tag{16a}$$

$$G_{2,\pm 1}^Q = 2g_{2,\mp 2}^Q(\mp 2\omega_0) + 3g_{2,\mp 1}^Q(\mp\omega_0) + 2g_{2,\pm 1}^Q(\pm\omega_0)$$
$$+ 3g_{2,0}^Q(0) \tag{16b}$$

where ω_0 is the Larmor frequency of the nucleus. The superscripts Q indicate that these expressions are specific for

quadrupolar relaxation. The $G_{l,m}^Q$ quantities are linear combinations of various spectral densities:

$$g_{l,m}(\omega) = \int_0^\infty f_{lm}(t) \exp(i\omega t)\, dt \tag{17}$$

The spectral densities are calculated as the (half-)Fourier transforms of the autocorrelation functions $f_{l,m}(t)$ of the irreducible EFG tensor components ($l = 2$),

$$\begin{aligned} f_{l,m}(t) &= (-1)^{(l+m)}\langle R_{l,-m}(t_0)R_{l,m}(t_0 - t)\rangle \\ &= (-1)^{(l+m)}\langle R_{l,-m}(t_0 + t)R_{l,m}(t_0)\rangle \\ &= \langle R_{l,m}(t_0)R_{l,m}^*(t_0 + t)\rangle \end{aligned} \tag{18}$$

In the previous expression, $R_{l,m}^* = (-1)^{(l+m)}R_{l,m}$. Furthermore, t_0 indicates some chosen time origin. A bracketed term $\langle \cdots \rangle$ denotes an ensemble average of the autocorrelation functions.

As written in eq 17, the spectral densities are functions of the frequency. Let τ be a characteristic correlation time for the various EFG tensor components, such that the $f_{l,m}$ vanish for t much larger than τ. A correlation time for the quadrupolar interaction can be defined via

$$\tau_{l,m} = \int_{t_0}^\infty \frac{\langle R_{l,m}(t_0)R_{l,m}^*(t_0 + t)\rangle}{\langle R_{l,m}(t_0)^2\rangle}\, dt \tag{19}$$

The relationship given above can be interpreted as the time required for EFG component to be largely uncorrelated with itself, or, in other words, the time needed for these components to lose the memory of the initial values computed at t_0. The physically observed relaxation time (the inverse of the relaxation rate) for a macroscopic sample is the time, after the exciting pulse, needed for the ensemble of nuclear spins to recover to equilibrium by transferring the absorbed energy to the bulk. For quadrupolar nuclei, the energy transfer is mediated dominantly by the quadrupole–EFG interaction. This process is determined by short-term microscopic phenomena such as the autocorrelation of the EFG fluctuations, and by the average inverse square of the quadrupolar interaction, since the variance of the EFG fluctuations (see below) and Q^2 enter the relaxation rate expressions. As shown in section 4, for systems with comparable microscopic correlation times, the observed relaxation times may vary by orders of magnitude, because of varying strengths of the quadrupolar interaction. Furthermore, the shorter the autocorrelation times, the greater the relaxation time, meaning that the energy transfer from the nuclear spins to the surrounding is less effective.

Under the condition of "extreme narrowing",[42] which is defined as $\omega\tau \ll 1$, the correlation time is so short that the product ωt in the exponent in eq 17 is effectively zero for time ranges where the autocorrelation functions can give contributions to the spectral densities. The extreme narrowing condition then corresponds to the calculation of the spectral densities at zero frequency. This approximation implies that the computed relaxation times are independent of the strength of the external magnetic field. Indeed, because of strong variation of the simulated correlation times (vide infra), keeping the exponential phase factor in eq 17 has a negligible influence on the computed NMR relaxation times. The validity of the extreme-narrowing regime, $\omega\tau \ll 1$ is explicitly tested in the code using a default field strength of 9 T, which can be changed upon input. For our samples, $\omega\tau \ll 1$ was found to be valid.

Table 1. Selected Structural and Dynamic Properties Computed from the aiMD Simulations of Alkali and Halide Ions in Water[a]

ion X	T_{avg} (K)	D_{H_2O} (Å²/ps)	$g_{max}(r_{X-O})$	$R_{max}(r_{X-O})$ (Å)	$g_{min}(r_{X-O})$	$R_{min}(r_{X-O})$ (Å)	ref
Li⁺	287 ± 12	0.0060	9.4 [8.5]	1.97 [1.96]	0.0 [0.0]	2.8 [2.8]	52
Na⁺	300 ± 13	0.0065	5.4 [3.6]	2.44 [2.49]	0.0 [0.5]	3.2 [3.2]	56
	T_{avg} (K)	D_{H_2O} (Å²/ps)	$g_{max}(r_{X-H})$	$R_{max}(r_{X-H})$ (Å)	$g_{min}(r_{X-H})$	$R_{min}(r_{X-H})$ (Å)	ref
Cl⁻	300 ± 14	0.0258	2.2 [2.6]	2.20 [2.18]	0.2 [0.2]	2.8 [2.9]	53
Br⁻	302 ± 15	0.0287	2.3 [1.8]	2.39 [2.35]	0.2 [0.3]	3.1 [3.1]	54
I⁻	286 ± 14	0.0125	1.9 [1.6]	2.53 [2.61]	0.2 [0.3]	3.2 [3.3]	55

[a]The average temperature (T_{avg}), the water diffusion coefficient (D_{H_2O}), the first maximum and minimum of relevant $g(r)$, along with the corresponding position R, have been calculated after the NVT equilibration step. Data given in brackets were obtained from the listed references.

One further point can be made for systems without rotational anisotropy.[36] In this case, the autocorrelation functions and the spectral densities $g_{l,m}$ in eqs 16 for different m should become equal. In the extreme narrowing limit (fast motion), one then has

$$g_{2,m}(\omega) = g_2(0)$$

$$G_{2,1}^Q(\omega) = G_{2,0}^Q(\omega) = G_2^Q(0) = 10g_2(0)$$

$$\frac{1}{T_1} = \frac{1}{T_2} = \frac{e^2 Q^2 (2I+3)}{40 I^2 (2I-1)\hbar^2} G_2^Q(0) \tag{20}$$

A common correlation time τ can be defined accordingly as any of the $\tau_{l,m}$, or, more practically in finite simulations, as their average.

In the DynPro implementation, the autocorrelation functions and corresponding time integrations are calculated numerically for a finite number n of time steps, as detailed in Section 4.1. In the code, we start from normalized autocorrelation functions calculated for a selected time origin t_0,

$$f'_{l,m}(t) = \frac{\frac{1}{n}\sum_{t_0=1}^{n-t} R_{l,m}(t_0) R_{l,m}^*(t_0+t)}{\frac{1}{n}\sum_{t_0=1}^{n} R_{l,m}(t_0) R_{l,m}^*(t_0)} = \frac{f_{l,m}(t)}{\sigma_{l,m}} \tag{21}$$

where $\sigma_{l,m}$ represents the variance of the spherical EFG tensor component l,m over the sample configurations, which are also stored independently. The variables t_0 and t count discrete time steps of the simulation. Under the condition $\omega_0 \to 0$, numerical time integration of these normalized autocorrelation functions gives accordingly normalized spectral density values $g'_{l,m}$, which are then multiplied by $\sigma_{l,m}$ and combined as in eqs 16 to give $G_{l,m}^Q$.

The quantity $\langle V(0)^2 \rangle$ reported later in section 44 is the sum of the variances:

$$\langle V(0)^2 \rangle = \sum_{m=-2}^{m=2} \sigma_{2,m} \tag{22}$$

The correlation times presented in section 4 are calculated as follows:

$$\tau = \frac{1}{\langle V(0)^2 \rangle} \sum_{m=-2}^{m=2} g_{2,m} \tag{23}$$

which is equal to the average of the $\tau_{2,m}$ terms given by eq 19, under the extreme narrowing condition and in the absence of rotational anisotropy. In this case, the relaxation rate of eq 20 is observed to be proportional to the product of the correlation time and the variance of the EFG tensor components. Hence, assuming all other factors are the same when comparing

different systems, the relaxation rate increases bilinearly with the correlation time and with $\langle V(0)^2 \rangle$. For a completely uncorrelated set of EFG data, one may therefore expect the relaxation rates to become very small. For numerically meaningful results, the correlation times must be much larger than the time intervals at which configuration snapshots are taken for the EFG calculations, and the time range used in eq 17 for the integration must be sufficiently large, such that the magnitude of the $f_{l,m}$ term falls below the numerical noise.

3. COMPUTATIONAL DETAILS

The general setup for the aiMD calculations and subsequent computations of molecular properties is similar to the protocol developed for refs 30−32, where the reader can find additional details. The aiMD were carried out with the Quantum-Espresso (QE) package.[29] In these simulations, the exchange correlation potential that was devised by Perdew, Burke, and Ernzerhof (PBE)[43,44] has been adopted. The aiMD simulation were performed with periodic boundary conditions, using cubic boxes containing 64 (or 63) water molecules, the ion of interest, and a proton (or OH⁻) to balance the charges. Therefore, the ion concentrations correspond to a molality of ~0.9 mol/kg. The box dimensions were adjusted to give a density of ~1 g/cm³. Ultrasoft pseudo-potentials were used for all atom species, and the convergence with respect to the kinetic energy cutoff of the plane wave basis has been checked. A value of 40 Ry was found to give an acceptable compromise between accuracy and efficiency. The aiMD simulations were performed with the Verlet algorithm, using a fictitious electron mass of 450 a.u. for the Car−Parrinello[45] procedure and a time step of 5.0 a.u. (corresponding to 0.121 fs). The total simulation times were in the range of 13−20 ps. Initial configurations were generated from aiMD samples of pure water. After having included the ion and balanced the charge accordingly, the atomic positions were optimized within fixed cell parameters, using a standard force minimization algorithm. Nuclear kinetic energy was then introduced by small increments during 1 ps of trajectory, using the velocity rescaling approach. Once the target effective temperature of 300 K was reached, the Nosé−Hoover thermostat chain[46,47] was used for simulations within the Canonical Ensemble.

Computation of the relaxation rates were performed after an equilibration phase of ~4 ps within the NVT ensemble, followed by 6 ps of further equilibration within the NVE ensemble. Test calculations for ^{81}Br⁻ were perfomed with 128, 256, 512, and 1024 aiMD "snapshot" configurations taken over sampling periods of 3.6, 4.8, 6.0, and 7.2 ps, in order to determine a suitable protocol (see Section 4.1). For the relaxation time calculations, 1024 configurations from a range

of 3.6 ps in a late stage of the aiMD trajectory has been used for all ions.

The accuracy and reliability of aiMD simulations are dependent on many technical parameters and on the quality of the electronic structure model (i.e., in our case, the density functional). This topic has been investigated in detail for liquid water (see, e.g., refs 48−50). The influence of the density functional recently has been investigated exhaustively.[51] In our work, the PBE was chosen for this initial proof of concept, mainly for reasons of continuity with our previous aiMD work on dynamical averaging of NMR parameters, where the PBE functional performed well.[30−32] In order to check the reliability of our simulations further, structural and dynamic properties computed from the NVE production runs are collected in Table 1. We also collect data extracted from previous simulations using the BLYP functional for Li^+, Cl^-, Br^-, and I^- in water,[52−55] and from a PBE simulation for Na^+.[56] The PBE functional somewhat overstructures the radial distribution functions (RDFs) compared to BLYP, but the agreement remains satisfactory, considering that computational details differ in many respects.

While a prediction of bulk properties of water is not a goal of this work, there is the possibility to assess the reliability of the aiMD simulations with the help of calculated diffusion coefficients D. The calculation of such a macroscopic observable is likely unreliable for the ions, because of the poor statistical representation. However, the water self-diffusion coefficients D_{H_2O} calculated from the mean-square-displacement (MSD) of the H_2O molecule center of mass is a good indicator for molecular dynamics reliability.[50] From the D_{H_2O} values reported in Table 1, we observe that the mobility of water molecules for solvated cations is reduced, compared to halides, which is tentatively associated with stronger interactions of the solute with the less polarizable and smaller cations. Compared to the D_{H_2O} data evaluated for pure liquid water, our results fall within the range of variation 0.005−0.05 $Å^2/ps$ that has been reported in the past.[48,50,51]

Calculations of EFG tensors were carried out using the Amsterdam Density Functional (ADF) suite of programs.[57−59] Scalar relativistic effects were treated by the Zeroth Order Regular Approximation (ZORA).[60] A triple-ζ Slater-type orbital basis set with two sets of polarization functions (TZ2P) from the ADF basis set library was employed for all atoms. The EFG tensors were computed with the revised PBE functional (revPBE),[61] and, in selected cases, with a hybrid version of PBE including 25% of exact nonlocal exchange (PBE0).[62] The EFG calculations employed ion−solvent clusters of varying size taken from configurations along the aiMD trajectory. An example taken from the aiMD simulation for $^{81}Br^-$ is shown in Figure 1 for illustration. The generation of clusters with a selected number of nearest solvent molecules, and the subsequent relaxation rate calculations, employed a modified version of the DynPro code that we developed as a utility module in the QE package. The calculation of the relaxation rates and correlation times has been carried out with the formalism described in section 2. In order to estimate statistical errors for the correlation times and relaxation rates, we calculated the standard deviations for $\langle V(0)^2 \rangle$. Furthermore, sets of random numbers with the same standard deviation and mean zero were generated to represent random fluctuations of the EFG tensor components. The random numbers were added to the calculated EFG tensors, followed by a re-evaluation of
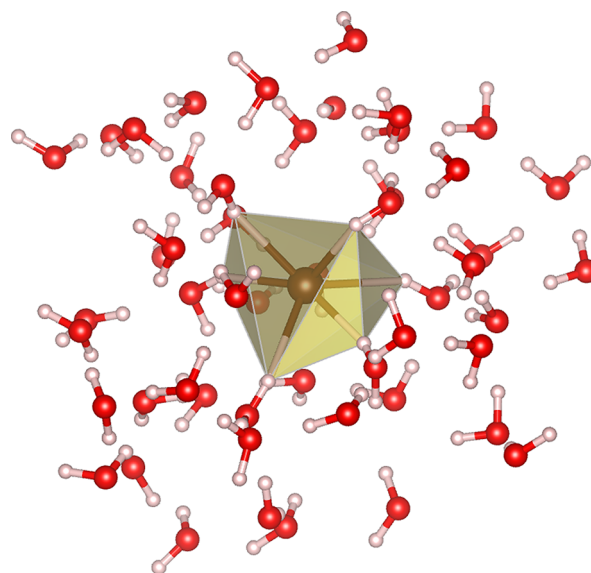

Figure 1. Snapshot from the aiMD simulation for $^{81}Br^-$ in water. The polyhedron indicates nearest solvent−ion contacts.

the relaxation rates and correlation times. The difference between the new and the original set of data was taken to represent a rough estimate of errors in the relaxation rates arising from random uncertainties in the calculated EFGs. Evidently, they not cover systematic errors from the electronic structure model, basis set truncation, aiMD accuracy constraints, and other approximations, which are major factors that influence the accuracy of the relaxation rate calculations.

4. RESULTS AND DISCUSSION

4.1. $^{81}Br^-$: Benchmarks and Protocol Development. In order to determine a protocol for aiMD-based quadrupolar relaxation rate calculations, we performed a range of test calculations for bromide. The $^{81}Br^-$ ion is easily polarizable; therefore, this system is expected to be quite sensitive to the simulation parameters (iodine more so, chlorine less so). The chemically "harder" Group 1 cations are less polarizable and expected to be somewhat less sensitive to approximations in the computational model. From prior work,[13,14] it is known that the corresponding correlation times τ are considerably lower than 1 ps. Therefore, relaxation rate calculations utilizing data from several picoseconds of aiMD simulation can be considered suitable for an initial assessment. As far as the electronic structure model in the EFG calculations is concerned, the combination of the TZ2P Slater-type basis and the PBE functional used for this work, and similar density functionals, have been shown to perform well for EFG calculations of main group atoms.[39,63,64] Accordingly, the protocol development can focus on several technical aspects, such as

(i) How much simulation time is needed to equilibrate the sample?

(ii) How many picoseconds of simulation time need to be covered for the relaxation rate calculation?

(iii) How many aiMD configurations are needed in the relaxation rate calculation?

(iv) Related to (ii) and (iii): How large or small should the time between aiMD snapshots be in order to determine the relaxation rates?

(v) How many water molecules need to be included in the QM EFG calculations?

While it is desirable to calculate the relaxation rates from the production phases of a large number of independent aiMD simulations with a large number of configurations over a considerable time frame, finite computational resources require suitable compromises. For the present work, the required data were obtained from single aiMD trajectories. We plan to investigate the benefit of using multiple independent trajectories in follow-up work.

Points (i) through (iv) were addressed by calculating the relaxation rates for $^{81}Br^-$ using varying numbers of aiMD configurations (128−1024) at varying time intervals along the dynamics as discussed below, after equilibration phases of ~10 ps. Based on an initial set of 1024 aiMD configurations between 9.6 ps and 16.8 ps (the available simulation range), EFG tensors were calculated for $^{81}Br^-$ with a small number of solvent molecules. To address point (v), a configuration with a particularly large magnitude of the EFG (V_{33}) was selected, and the convergence with respect to the number of solvent molecules was investigated. Figure 2 shows the convergence
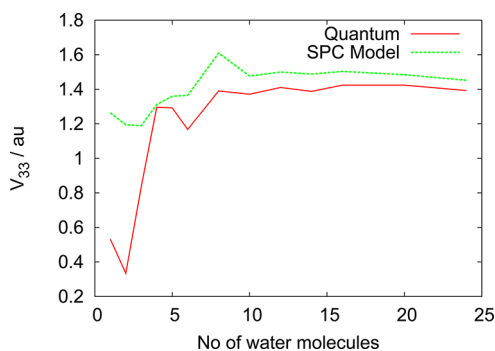

Figure 2. Dependence of the principal component V_{33} of the $^{81}Br^-$ EFG of a selected aiMD configuration on the number of surrounding water molecules treated quantum mechanically. "SPC" indicates the presence of up to 2×10^3 additional water molecules represented by point charges.

of the EFG with the number of solvent molecules treated at the quantum mechanical level. In addition to bare clusters, the calculations were repeated with a $3 \times 3 \times 3$ supercell of the simulation box, with the specified number of nearest water molecules treated quantum mechanically, and the remainder of the 1728 (= $3 \times 3 \times 3 \times 64$) water molecules represented by a point-charge model[65] in a type of MM embedding. With small

numbers of explicit solvent molecules included in the QM part of the model, the performance of the combined QM/MM embedding is clearly superior. However, with more than 10 water molecules, the convergence of the EFG is seen to be very similar with the two sets of calculations, with convergence being reached approximately at ~16 water molecules. To keep the setup of the calculations simple, the remainder of the computations discussed herein utilized solvent−solute clusters containing the ion of interest and 20 explicit water molecules at the QM level.

Radial distribution functions (RDFs) for oxygen and hydrogen atoms around the $^{81}Br^-$ ion are shown in Figure 3, along with the integrals as a function of the distance to bromide. A clear solvent structure is seen, with the number of atoms in the first large peak of both RDFs integrating up to ~6. These numbers indicate that Br···H−O−H interactions dominate the picture. When the number of hydrogens within a distance of 4 Å is plotted as a function of time, the result oscillates at ~12 (corresponding to six waters). Figure 4 shows the corresponding plots for H and O, as well as plots for H with smaller cutoff distances. The plots reveal no clear correlation or anticorrelation between the number of coordinating solvent atoms and the induced EFG. This is likely due to the fact that the magnitude of the EFG, to a large degree, is driven by the dissymmetry of the nearest-neighbor interactions and not simply by the number of coordinating atoms.

Table 2 displays averages and standard deviations for the absolute values of the diagonal components of the EFG tensor, V_{xx}, V_{yy}, and V_{zz}, calculated from 1024 aiMD configurations for the indicated time intervals. For an isotropic system, the averages should be equal. Because of the limited duration of the aiMD simulations, these conditions are not satisfied. There is no clear trend, with respect to the different time intervals. Visual inspection of the molecular motions during the aiMD showed that, for instance, exchange of water molecules between solvent shells and rotational motions are slow processes that would require very long simulations to average out.[66] Yet, from the known relaxation rates, one can infer that the EFG autocorrelation time is on the order of 1 ps or less. Although it would be desirable to run simulations that fully establish the isotropic nature of the solution, we infer from the data discussed below that a nonisotropic finite-time simulation of the ion−solvent interactions incorporates an important part of the required information needed for the relaxation rate calculations.

Table 3 collects results from relaxation rate calculations for bromide over the different time ranges considered in Table 2,
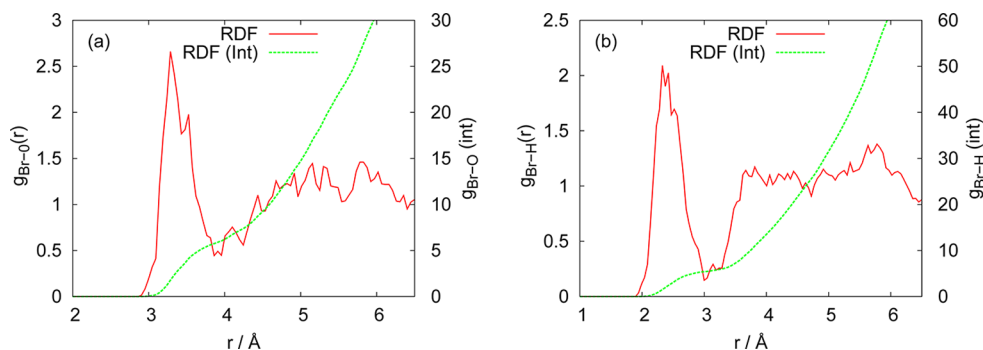

Figure 3. (a) Br−O and (b) Br−H radial distribution functions (RDFs, red) for $^{81}Br^-$ in water, calculated from 1024 configurations in the 13.3−16.9 ps simulation range. Integrated RDFs (green) are also shown.
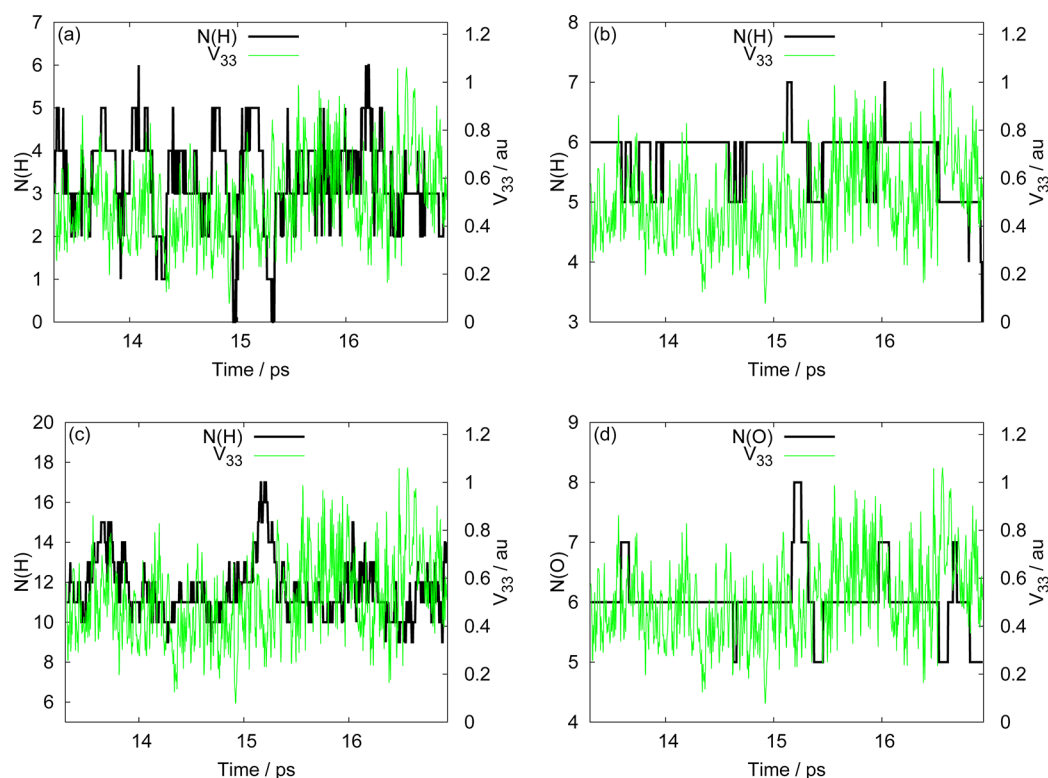
Figure 4. Variation of V_{33} (green) and the number of hydrogen or oxygen atoms, $N(H)$ or $N(O)$, within a different cutoff radius versus time: (a) $N(H)$, $r_{cut} = 2.5$ Å; (b) $N(H)$, $r_{cut} = 3.0$ Å; (c) $N(H)$, $r_{cut} = 4.0$ Å; and (d) $N(O)$, $r_{cut} = 4.0$ Å.

Table 2. Absolute Averages and Standard Deviations (σ) for the Diagonal Cartesian Components of the $^{81}Br^-$ EFG Tensor during Selected Time Intervals of the aiMD Simulation (a.u.)

time range (ps)	$|V_{xx}|$	$\sigma_{|V_{xx}|}$	$|V_{yy}|$	$\sigma_{|V_{yy}|}$	$|V_{zz}|$	$\sigma_{|V_{zz}|}$
9.6−16.9	0.192	0.236	0.300	0.244	0.311	0.236
10.9−16.9	0.188	0.231	0.308	0.241	0.304	0.235
12.1−16.9	0.185	0.228	0.320	0.251	0.318	0.231
13.3−16.9	0.192	0.234	0.314	0.261	0.311	0.220

Table 3. Quadrupolar Relaxation Rate of $^{81}Br^-$ in Aqueous Solution, Covering Different Time Ranges of the aiMD Simulation (1024 Configurations Each)[a]

time range (ps)	$\langle V(0)^2 \rangle$ (a.u.)	τ (ps)	$1/T_1$ (s^{-1})	$1/T_2$ (s^{-1})
9.6−16.9	0.598(11)	0.886(99)	2166(55)	6817(86)
10.9−16.9	0.577(12)	0.260(32)	2364(25)	1055(22)
12.1−16.9	0.620(11)	0.589(66)	1709(13)	4586(30)
13.3−16.9	0.610(11)	0.397(42)	977(66)	3122(99)

[a]Estimates for errors from random EFG variations in parentheses.

Table 4. Quadrupolar Relaxation Rate of $^{81}Br^-$ in Aqueous Solution, Covering Constant Time Ranges along the Trajectory of the aiMD Simulation (1024 Configurations Each)[a]

time range (ps)	$\langle V(0)^2 \rangle$ (a.u.)	τ (ps)	$1/T_1$ (s^{-1})	$1/T_2$ (s^{-1})
9.6−13.3	0.584(11)	0.390(49)	388(15)	3200(99)
10.9−14.5	0.572(10)	0.332(37)	1244(5)	2213(12)
12.1−15.7	0.543(08)	0.334(38)	843(6)	2279(6)
13.3−16.9	0.610(11)	0.397(42)	977(66)	3122(99)

[a]Estimates for errors from random EFG variations in parentheses.

using 1024 sampling points. In addition to the relaxation rates, the table provides the sum of the fluctuation (variance) of the EFG spherical components $\langle V(0)^2 \rangle$ and the correlation times defined in eq 23. In agreement with the data in Table 2, the EFG variances are close to each other for the different time ranges. However, the actual relaxation rates vary considerably. Table 4 provides a different view at the trajectory. Here, constant-width partially overlapping time windows were chosen to calculate the relaxation data. In both Tables 3 and 4, there is a considerable difference between $1/T_1$ and $1/T_2$, confirming the presence of rotational anisotropy already indicated by the

data in Table 2. The difference between $1/T_1$ and $1/T_2$ is particularly large for the earliest time window in Table 4. Correspondingly, we decided that data collection for the relaxation rate calculation should be taken after ~12 ps of simulation, and that a sampling window of several picoseconds is needed at the very minimum. Correspondingly, for $^{81}Br^-$ and the other ions, a time window of ~3.6 ps from the latest segment of the simulations was employed to calculate relaxation rates. The differences between $1/T_1$ and $1/T_2$ are large enough such that error estimates from random fluctuations in the EFGs from sampling over only a few hundred up to 1024 configurations is a secondary concern. Below, we compare results from eqs 20 with the experiment. The key quantity, $g_2(0)$, is, in this case, calculated from an *average* of the $g_{2,m}(0)$, which provides an approximate isotropic average for the relaxation rate that the aiMD itself is too short to deliver.

The decay of the autocorrelation functions (ACFs) f_{20}, f_{21}, and f_{22} for the fluctuating EFG of $^{81}Br^-$ in aqueous solution over the 3.6 ps time window is shown in Figure 5. The decay of the function f_{20} is much slower than for other two ACFs. The
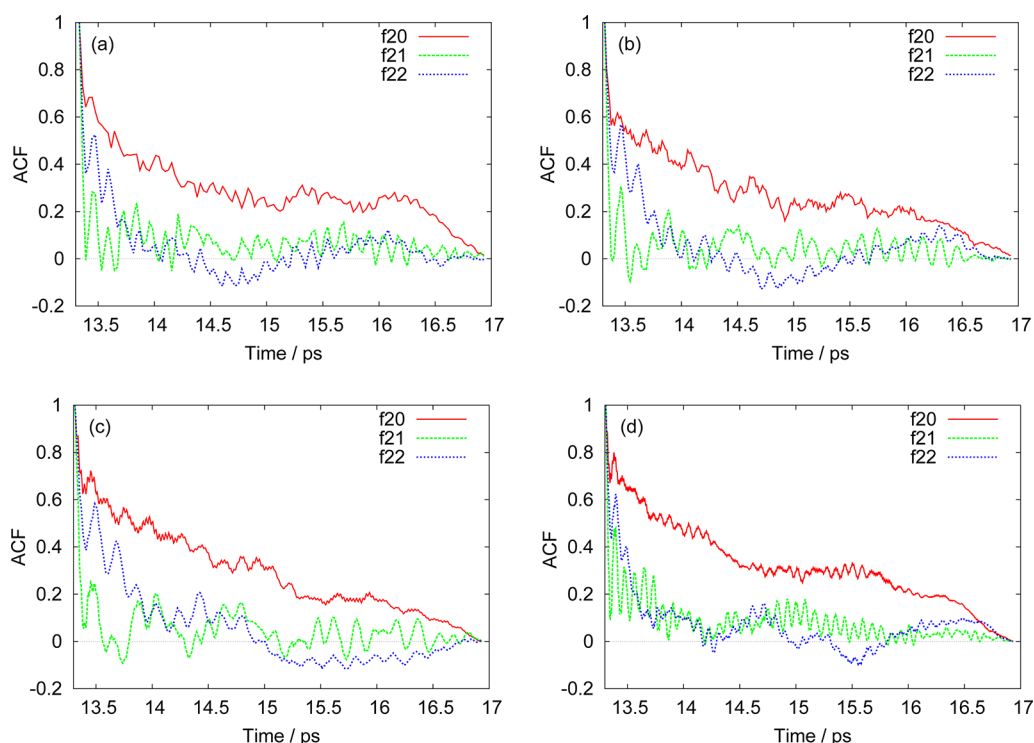
Figure 5. Autocorrelation function for sample size (a) 128, (b) 256, (c) 512, and (d) 1024 configurations for the EFG of $^{81}Br^-$ in water taken over the same time range.

functions f_{21} and f_{22} decay very fast in the first 0.5 ps and then approach zero more slowly. The region of fast decay is known as the libration region, whereas the region of slower decay is the main contributor to the relaxation rate.[28] As already noted in ref 28 (for proton and ^{17}O EFGs), the aiMD-derived ACFs appear very different from simple exponential functions. The differences between the $f_{2,m}$ for different m are due to the presence of the aforementioned rotational anisotropy. The effect from increasing the number of points in the numerical grid used to calculate the autocorrelation functions, for this particular sample, is seen to be relatively minor for f_{20}. While smaller details are exposed with the finer grid, the integration per eq 17 for $\omega = 0$ can be expected to give similar results. The changes with grid size for f_{22} and, in particular, for f_{21} are more pronounced. The corresponding calculated relaxation rate data, collected in Table 5, do indeed exhibit noticeable changes in

Table 5. Computational Results for Relaxation Rate of $^{81}Br^-$ in Aqueous Solution Calculated over the Time Interval from 13.3 ps to 16.9 ps with Different Numbers of Sampling Configurations (Also See Figure 5)

sample size	$\langle V(0)^2 \rangle$ (a.u.)	τ (ps)	$1/T_1$ (s^{-1})	$1/T_2$ (s^{-1})
128	0.620(32)	0.547(58)	1335(14)	4376(131)
256	0.610(23)	0.540(48)	1383(59)	4248(196)
512	0.610(15)	0.497(47)	1221(63)	3902(236)
1024	0.610(11)	0.397(42)	977(66)	3122(99)

the correlation times and relaxation rates as the sampling grid becomes denser. The changes in the data when going from 512 to 1024 points must clearly be related to the alterations of f_{22} and f_{21} seen in Figure 5d versus Figure 5c. Based on this analysis, we consider a sample of 1024 points to be a minimum requirement for generating suitable autocorrelation functions.

More points would evidently be better. Given the overall agreement of the relaxation rates in comparison with experiment, however, this would constitute a case of increasing precision without increasing accuracy. Therefore, we proceed with sample sizes of 1024.

For the 3.6 ps window underlying the data of Table 5 and Figure 5, relaxation rates were also calculated using batches of 256 sampling points out of the 1024 total (see Table 6). Given

Table 6. Bromide in Aqueous Solution: Relaxation Rate Data for Sample Sizes of 256 Points within Segments of the 13.3–16.9 ps Window

time range (ps)	$\langle V(0)^2 \rangle$ (a.u.)	τ (ps)	$1/T_1$ (s^{-1})	$1/T_2$ (s^{-1})
13.3–14.2	0.538(15)	0.169(20)	712(4)	1003(6)
14.2–15.1	0.396(14)	0.049(06)	83(1)	246(27)
15.1–16.0	0.653(20)	0.128(15)	334(12)	1074(27)
16.0–16.9	0.851(26)	0.182(16)	1209(47)	1699(48)

the behavior of the ACFs shown in Figure 5, it is evident that these time windows are too small for a relaxation rate sampling. The averages of the relaxation rates from the 4 batches of 256 sampling points are also not suitable, as they differ considerably from those obtained from the calculations using the full set of 1024 points.

In summary, we find reasonable agreement (within a factor of ~2) with the experiment for the average of the $1/T_1$ and $1/T_2$ relaxation rates of $^{81}Br^-$ in aqueous solution, and, given the presence of rotational anisotropy, fortuitously good agreement for $1/T_1$, for (i) sampling of several ps starting after roughly 13 ps of aiMD simulation, (ii) using at least 1024 sampling points, and (iii) using upward of 15 nearest water molecules in the EFG calculations. A similar protocol has been adopted for
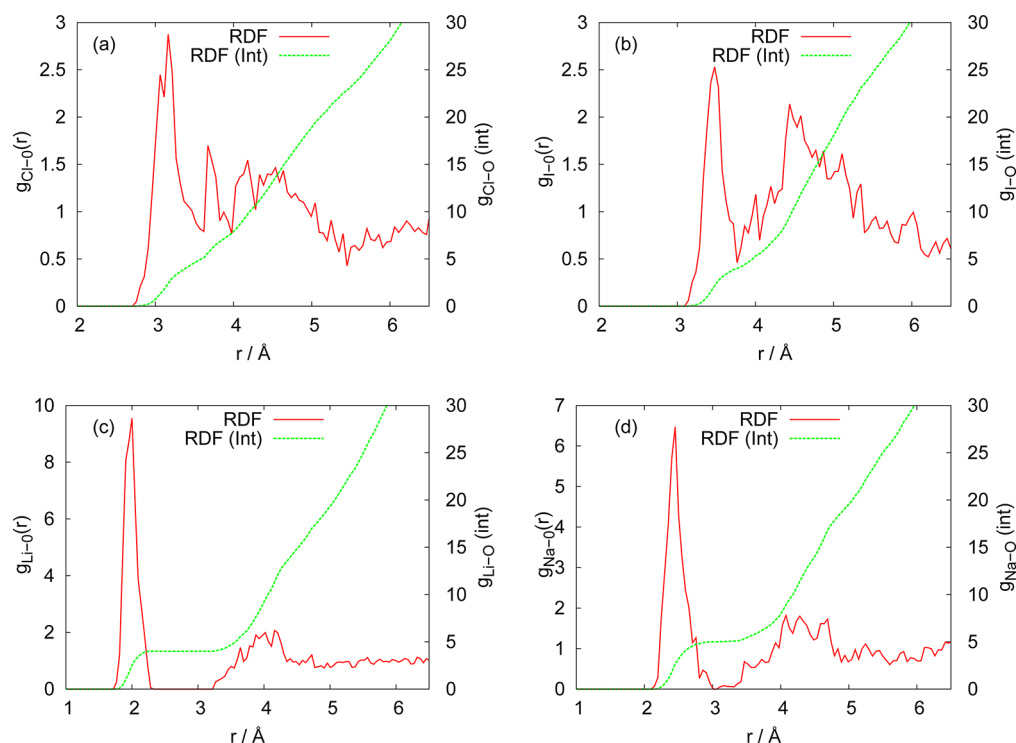
Figure 6. (a) Cl−O, (b) I−O, (c) Li−O and (d) Na−O RDFs (from 1024 aiMD configurations within the time intervals shown in Figure 8). The integrated RDFs (green) are also shown.
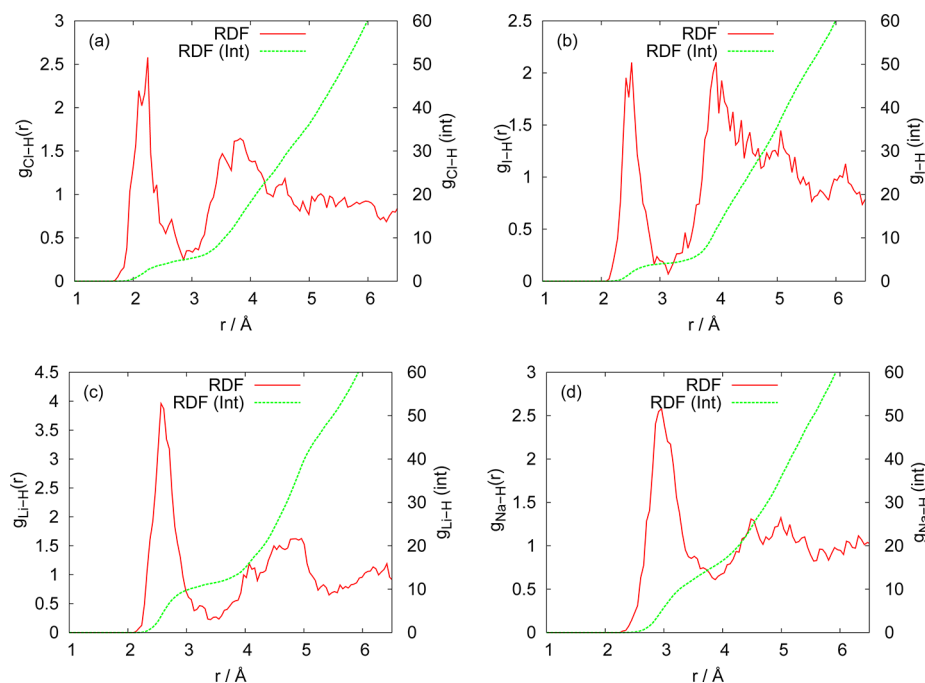

Figure 7. (a) Cl−H, (b) I−H, (c) Li−H and (d) Na−H RDFs (from 1024 aiMD configurations within the time intervals shown in Figure 8). The integrated RDFs (green) are also shown.

calculations of the relaxation rates of the other ions in aqueous solution.

4.2. Cl⁻, I⁻, Li⁺ and Na⁺. In this subsection, the results for the remaining ions in the test set—^{35}Cl⁻, ^{127}I⁻, ^{7}Li⁺, ^{23}Na⁺— are presented and discussed. The ion-oxygen and ion-hydrogen RDFs are shown in Figures 6 and 7, respectively. From the radial distributions, the first solvation shells are found to be in the range of 2.75−3.56 Å for chlorine, 3.14−3.75 Å for iodine,

1.77−2.28 Å for lithium, and 2.14−2.95 Å for sodium. The corresponding average coordination numbers, from integrating the first peak of the O-ion RDFs, are 5.1, 4.0, 4.0, and 5.0, respectively. For ^{23}Na⁺, the number of molecules in the first solvation shell is similar to what has been reported in ref 25.

The EFG ACFs, similar to Figure 5 for ^{81}Br⁻, are presented in Figure 8. The decaying trends for the ACFs appear qualitatively similar to those for ^{81}Br⁻, with steep initial drops
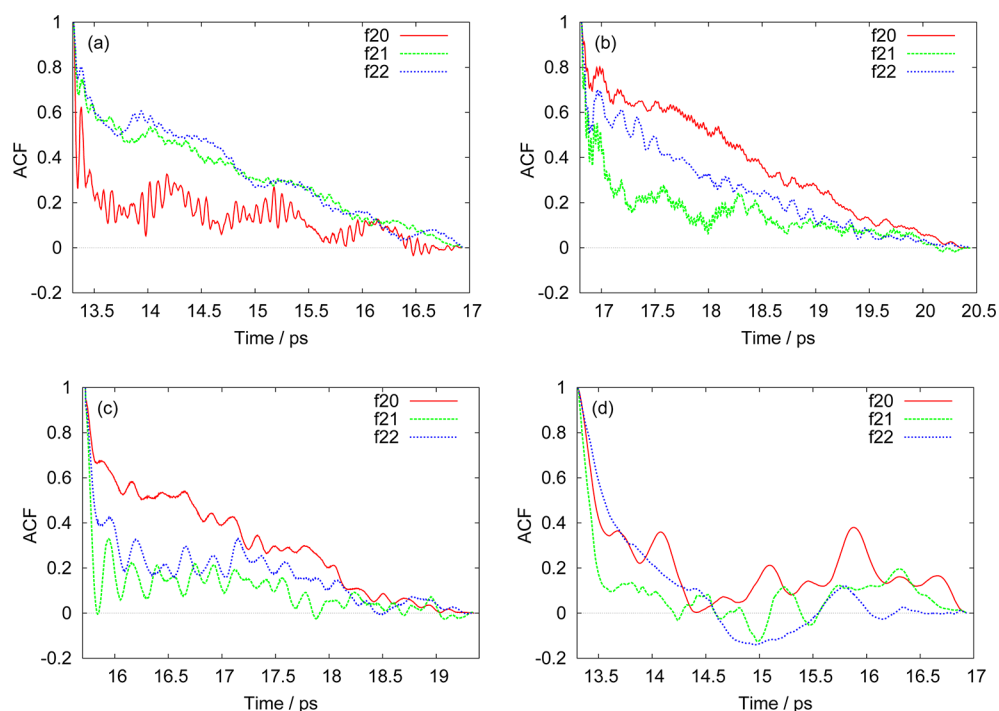
Figure 8. Autocorrelation functions for the EFG spherical tensor components of the respective ion in aqueous solution: (a) ^{35}Cl$^-$, (b) ^{127}I$^-$, (c) ^{7}Li$^+$, and (d) ^{23}Na$^+$.

Table 7. EFG Fluctuation, Correlation Time, and Relaxation Rates for All Ions, and Comparison with Experiment[a]

ion	$\langle V(0)^2 \rangle$ (a.u.)	τ (ps)	$1/T_1$ (s^{-1})	$1/T_2$ (s^{-1})	$1/T_{iso}$ (s^{-1})	$1/T_1$, exp (s^{-1})[b]
^{7}Li$^+$	$4.19(15) \times 10^{-4}$	0.508(44)	$3.58(3) \times 10^{-2}$	$5.67(18) \times 10^{-2}$	$4.97(14) \times 10^{-2}$	2.70×10^{-2}
^{23}Na$^+$	$3.11(6) \times 10^{-2}$	0.284(29)	14.12(15)	13.76(13)	13.88(14)	16.2
^{35}Cl$^-$	0.313(5)	0.368(39)	$1.43(1) \times 10^2$	96(1)	112(1)	29.2
^{81}Br$^-$	0.610(11)	0.397(42)	$9.77(7) \times 10^2$	$3.12(10) \times 10^3$	$2.41(9) \times 10^3$	1.05×10^3
^{127}I$^-$	1.70(27)	0.638(70)	$1.52(3) \times 10^4$	$1.99(8) \times 10^4$	$1.83(6) \times 10^4$	4.60×10^3

[a]Data taken from ref 14. [b]The field strength was not specified in ref 14. The spectrometer model used for the experimental observations likely had a 2.1 T magnet.[67]

over a short sampling period followed by a gradual decline. As noted for ^{81}Br$^-$, the ACFs do not appear to exhibit exponential decay.

Table 7 provides a comparison for the relaxation rates of all ions considered for this work with experimental data from ref 14. The computed data are based on a single aiMD trajectory each, using the sampling windows as indicated in the plots of the ACFs in Figure 8. Relaxation rates, calculated from eqs 20, that apply to cases without rotational anisotropy are also presented in Table 7; these data are indicated as $1/T_{iso}$.

For ^{23}Na$^+$, the results were found to vary considerably with the chosen sampling range of the aiMD trajectory. For instance, the $1/T_1$ relaxation rates obtained from sampling in the time intervals of 9.6−13.2, 13.3−16.9, and 16.8−20.4 ps were 4.0, 14.1, and 38.7 s^{-1}, respectively. The 14.1 value, as well as the average of the three samples are reasonably close to the experimental results. The rates $1/T_2$ and $1/T_{iso}$ are very similar for ^{23}Na$^+$, although some differences in the autocorrelation functions (Figure 8) show that the simulation length does not permit a fully isotropic sampling. The findings indicate that more-reliable estimates should be obtained from sampling over longer time ranges and using multiple independent aiMD trajectories.

Roberts and Schnitker[13] previously investigated Group 1 and Group 17 ions, as well as selected additional ions with classical MD simulations, using the SPC model for water, ion−water pair potentials, and semiempirical Sternheimer factors[68] to describe the EFG from the ion polarization. Correlation times τ for the EFG on the order of a few tenths of a picosecond obtained in the present work are consistent with those obtained in ref 13. The time ranges over which the ACFs decay to effectively zero are likewise consistent for the Group 17 anions. Plots for the Group 1 cation ACFs in ref 13 showed a somewhat larger time range of decay (reaching 6 ps) but with small magnitudes beyond 4 ps. The relaxation rates for ^{35}Cl$^-$, ^{81}Br$^-$, and ^{127}I$^-$ were overestimated in ref 13, by a factor of 2, with respect to experiment, while those for ^{7}Li$^+$ and ^{23}Na$^+$ were underestimated. The very different methodology used for the present work produces an overestimation for ^{7}Li$^+$ and a slight underestimation for ^{23}Na$^+$ and consistently overestimates the relaxation rates for the halides, overall not unlike the trends in ref 13. We note that the ACFs in the cited reference were based on a sum of products of Cartesian EFG tensor elements, while our work and the study in ref 28 employed the combinations of spherical tensor elements per eqs 16.

For ^{7}Li$^+$, ^{23}Na$^+$, and ^{81}Br$^-$, the computations produce the correct order of magnitude for the relaxation rates, within a

factor of ~3 from the experimental results. Overall, the relaxation rates span more than 5 orders of magnitude, but with similar underlying correlation times for the EFG tensor components. The cases of $^{35}Cl^-$ and $^{127}I^-$ agree less well with the experiment. For $^{35}Cl^-$, the calculated $1/T_1$ rate is too large, by a factor of 4.9. Using the equations for $1/T_2$ and for the isotropic case lowers the relaxation rate and brings the results closer to the experimental results, albeit with a considerable remaining overestimation. Table 8 provides some data for $^{35}Cl^-$

Table 8. PBE0 vs revPBE Results for $^{35}Cl^-$ with a Sample Size of 256

functional	$\langle V(0)^2 \rangle$ (a.u.)	τ (ps)	$1/T_1$ (s^{-1})	$1/T_2$ (s^{-1})
revPBE	0.308	0.647	246	166
PBE0	0.257	0.646	206	138

taken with a smaller set of 256 configurations, showing that the EFG fluctuations and the relaxation rates are somewhat reduced when the PBE0 hybrid density functional is used instead of the nonhybrid functional revPBE. Although the change is not dramatic, it goes in the right direction. The iodine $\left(^{127}I^-\right)$ value for $1/T_1$ is borderline; the $1/T_2$ and $1/T_{iso}$ values are even larger. During the course of this study, we noted that the $^{127}I^-$ relaxation rate decreased as the simulation time was extended. Therefore, this system is likely to require additional simulation time. Iodine is easily polarizable, which causes particularly large "intrinsic" fluctuating EFG from fluctuating electron density polarizations of the ion, as is evident from the data in Table 7. Iodine has a particularly large quadrupolar Sternheimer factor,[68] which is about twice that of $^{81}Br^-$ and almost 5 times that of $^{35}Cl^-$. With a suitable computational protocol in place, we plan to address the cases of $^{127}I^-$ and $^{35}Cl^-$ in more detail in a follow-up study by using multiple aiMD trajectories and a selection of hybrid density functionals.

When comparing the cations and anions, the variances of the fluctuating EFGs are seen to differ considerably. The large and easily polarizable anions exhibit, as expected, large EFG fluctuations, whereas the chemically "hard" cations have accordingly much smaller $\langle V(0)^2 \rangle$ values (Table 7). As discussed in section 2, within the framework of approximations adopted, the relaxation rates are proportional to the correlation times and to the magnitude of the EFG variances. Furthermore, the relaxation rates are proportional to the square of the nuclear quadrupole moment. As already pointed out, the correlation times for the different systems are comparable, with variations of a factor of ~2. The EFG fluctuations increase by a nearly 4 orders of magnitude when going from $^7Li^+$ to $^{127}I^-$. The quadrupole moments Q vary as follows:[41] $^7Li^+ = -40$ mbarn, $^{23}Na^+ = 104$ mbarn, $^{35}Cl^- = -82$ mbarn, $^{81}Br^- = 262$ mbarn, $^{127}I^- = -696$ mbarn. Therefore, Q^2 covers more than 2 orders of magnitude within the set of ions. The variations in Q^2 and $\langle V(0)^2 \rangle$ values therefore explain the range of more than 5 orders of magnitude for the resulting relaxation rates.

The required sampling times for the relaxation rate calculations are likely to depend on the type of system that is modeled. For instance, Schmidt et al.[28] used on the order of 35 ps of aiMD simulation time for calculating proton and ^{17}O relaxation times in liquid water, to obtain T_1 relaxation times within a factor of ~3 from the experiment. The authors noted that this margin of agreement can be taken as a "strong confirmation that the fundamental physical processes are correctly described" by the aiMD simulations. Our data are in

comparable agreement with experiment as those of ref 28. Moreover, despite the fact that the conversion of the EFG autocorrelation functions to relaxation times produces results in the millisecond regime or longer, it was noted in ref 28 that such physical phenomena can be modeled with aiMD simulations on time scales of 10^1 ps. The present results for the vastly differing relaxation rates of the Group 1 and Group 17 ions corroborate this finding.

5. CONCLUSIONS AND OUTLOOK

Ab initio molecular dynamics (aiMD) has been applied to compute NMR quadrupolar relaxation rates for closed-shell singly charged Group 1 and Group 17 ions ($^7Li^+$, $^{23}Na^+$, $^{35}Cl^-$, $^{81}Br^-$, and $^{127}I^-$). The Car−Parrinello aiMD simulations covered a range of ~20 ps and were deemed sufficiently well equilibrated for data sampling after 12−13 ps of simulation time. Electric field gradient (EFG) tensors were computed for ion-solvent clusters with an external quantum chemistry program. The relaxation rates are determined by EFG tensor element autocorrelations with correlation times on the order of 0.5 ps, in agreement with a previous classical MD study. Moreover, the magnitude of the relaxation rate is driven by the variance $\langle V(0)^2 \rangle$ of the induced fluctuating EFG at the ion's nucleus, ranging from 10^{-4} a.u. to 2 a.u. The short correlation times justify the approximations for the extreme narrowing limit. The calculated relaxation rates are in reasonable agreement with the experiment ($^{35}Cl^-$ and $^{127}I^-$ are borderline cases). As has been already pointed out in a previous aiMD study of ^{17}O and ^2H quadrupolar relaxation rates in liquid water,[28] the fact that the correct orders of magnitude are obtained with the calculations is an indication that the underlying physical description of the systems correctly describes the main factors driving the relaxation process.

The quality of the results can likely be improved by increasing the simulation times, allowing for a longer time window for sampling the EFGs with a larger number of data points, and by considering several independent aiMD trajectories. Furthermore, although preliminary results for $^{35}Cl^-$ obtained for the present work do not indicate a strong dependence of the calculated EFG tensors on the chosen functional (PBE vs PBE0), the reduction of the fluctuating EFG changes the relaxation rates in the desired direction. It appears worthwhile to perform a broader test of density functionals for several different cations and anions. In the light of recent comparisons of different DFT-based aiMD approaches to describe the liquid water structure,[51] it will also be interesting to test the dependence on the functional used for the dynamics. Work along these lines is currently underway in our laboratory.

■ AUTHOR INFORMATION

Corresponding Author
*E-mail: jochena@buffalo.edu.

Notes
The authors declare no competing financial interest.

■ ACKNOWLEDGMENTS

■ REFERENCES

(1) Kowalewski, J.; Mäler, L. *Nuclear Spin Relaxation in Liquids: Theory, Experiments, and Applications*; Taylor & Francis: New York, 2006.

(2) Hanni, M.; Lantto, P.; Vaara, J. *Phys. Chem. Chem. Phys.* **2011**, *13*, 13704−13708.

(3) Lindgren, M.; Laaksonen, A.; Westlund, P.-O. *Phys. Chem. Chem. Phys.* **2009**, *11*, 10368−10376.

(4) Bühl, M.; Parrinello, M. *Chem.—Eur. J.* **2001**, *7*, 4487−4494.

(5) Bühl, M.; Grigoleit, S.; Kabrede, H.; Mauschick, F. T. *Chem.—Eur. J.* **2006**, *12*, 477−488.

(6) Bühl, M. *Annu. Rep. NMR Spectrosc.* **2008**, *64*, 77−125.

(7) Autschbach, J.; Sterzel, M. *J. Am. Chem. Soc.* **2007**, *129*, 11093−11099.

(8) Zheng, S.; Autschbach, J. *Chem.—Eur. J.* **2011**, *17*, 161−173.

(9) Bloembergen, N.; Purcell, E. M.; Pound, R. V. *Phys. Rev.* **1948**, *73*, 679−712.

(10) Solomon, I. *Phys. Rev.* **1955**, *99*, 559−565.

(11) Redfield, A. G. *IBM J. Res. Dev.* **1957**, *1*, 19−31.

(12) Chen, S. W. W.; Rossky, P. J. *J. Phys. Chem.* **1993**, *97*, 10803−10812.

(13) Roberts, J. E.; Schnitker, J. *J. Phys. Chem.* **1993**, *97*, 5410−5417.

(14) Weingärtner, H.; Hertz, H. G. *Ber. Bunsen−Ges.* **1977**, *81*, 1204−1221.

(15) Deverell, C.; Frost, D. J.; Richards, R. E. *Mol. Phys.* **1965**, *9*, 565−577.

(16) Hertz, H. G. *Ber. Bunsen−Ges.* **1973**, *77*, 531−540.

(17) Hertz, H. G. *Ber. Bunsen−Ges* **1973**, *77*, 688−697.

(18) Endom, L.; Hertz, H. G.; Thul, B.; Zeidler, M. D. *Ber. Bunsen−Ges.* **1967**, *71*, 1008−1031.

(19) Hertz, H. G.; Holz, M.; Klute, R.; Stalidis, G.; Versmold, H. *Ber. Bunsen−Ges.* **1974**, *78*, 24−35.

(20) Borthakur, A.; Mellon, E.; Niyogi, S.; Witschey, W.; Kneeland, J. B.; Reddy, R. *NMR Nanomed.* **2006**, *19*, 781−821.

(21) Madelin, G.; Jerschow, A.; Regatte, R. R. *NMR Biomed.* **2012**, *25*, 530−537.

(22) Ooms, K. J.; Cannella, M.; Vega, A. J.; Marcolongo, M.; Polenova, T. *Magn. Reson. Med.* **2008**, *60*, 246−252.

(23) Kemp, D. D.; Gordon, M. S. *J. Phys. Chem. A* **2008**, *112*, 4885−4894.

(24) Jorgensen, W. L.; Chandrasekhar, J.; Madura, J. D.; Impey, R. W.; Klein, M. L. *J. Chem. Phys.* **1983**, *79*, 926−935.

(25) Aidas, K.; Ågren, H.; Kongsted, J.; Laaksonen, A.; Mocci, F. *Phys. Chem. Chem. Phys.* **2013**, *15*, 1621−1631.

(26) Lucken, E. A. C. *Nuclear Quadrupole Coupling Constants*; Academic Press: New York, 1969.

(27) Izvekov, S.; Voth, G. A. *J. Chem. Phys.* **2002**, *116*, 10372−10376.

(28) Schmidt, J.; Hutter, J.; Spiess, H.-W.; Sebastiani, D. *ChemPhysChem* **2008**, *9*, 2313−2316.

(29) Quantum-ESPRESSO is a community project for high-quality quantum-simulation software, based on density functional theory, and coordinated by Paolo Giannozzi. See http://www.quantum-espresso.org and http://www.pwscf.org (accessed July 2013).

(30) Sutter, K.; Truflandier, L. A.; Autschbach, J. *ChemPhysChem* **2011**, *12*, 1448−1455.

(31) Truflandier, L. A.; Autschbach, J. *J. Am. Chem. Soc.* **2010**, *132*, 3472−3483.

(32) Truflandier, L. A.; Sutter, K.; Autschbach, J. *Inorg. Chem.* **2011**, *50*, 1723−1732.

(33) Lucken, E. A. C. *Tetrahedron* **1963**, *19*, 123−41.

(34) Slichter, C. *Principles of Magnetic Resonance*; Springer−Verlag: New York, 1990.

(35) Spiess, H. W. Rotation of Molecules and Nuclear Spin Relaxation. In *NMR Basic Principles and Progress*, Vol. *15*; Diehl, P.; Fluck, E.; R. K., Ed.; Springer: Berlin, 1978; pp 55−214.

(36) Cowan, B. *Nuclear Magnetic Resonance and Relaxation*; Cambridge University Press: Cambridge, U.K., 2005.

(37) Wasylishen, R. Characterization of NMR tensors via experiment and theory. In *Calculation of NMR and EPR Parameters. Theory and Applications*; Kaupp, M., Bühl, M., Malkin, V. G., Eds.; Wiley−VCH: Weinheim, Germany, 2004; pp 433−447.

(38) Bryce, D. L.; Sward, G. D. *Magn. Reson. Chem.* **2006**, *44*, 409−450.

(39) Autschbach, J.; Zheng, S.; Schurko, R. W. *Concepts Magn. Reson. A* **2010**, *36A*, 84−126.

(40) Perras, F. A.; Widdifield, C. M.; Bryce, D. L. *Solid State Nucl. Magn. Reson.* **2012**, *45−46*, 36−44.

(41) Pyykkö, P. *Mol. Phys.* **2008**, *106*, 1965−1974.

(42) Abragam, A. *Principles of Nuclear Magnetism*; Oxford University Press: Oxford, 1961.

(43) Perdew, J. P.; Burke, K.; Wang, Y. *Phys. Rev. B* **1996**, *54*, 16533−16539.

(44) Perdew, J. P.; Burke, K.; Ernzerhof, M. *Phys. Rev. Lett.* **1998**, *80*, 891.

(45) Car, R.; Parrinello, M. *Phys. Rev. Lett.* **1985**, *55*, 2471−2474.

(46) Hoover, W. G. *Phys. Rev. A* **1985**, *31*, 1695−1697.

(47) Nosé, S. J. *Chem. Phys.* **1984**, *81*, 511−519.

(48) Grossman, J. C.; Schwegler, E.; Draeger, E. W.; Gygi, F.; Galli, G. *J. Chem. Phys.* **2004**, *120*, 300−311.

(49) Schwegler, E.; Grossman, J. C.; Gygi, F.; Galli, G. *J. Chem. Phys.* **2004**, *121*, 5400−5409.

(50) Lee, H.-S.; Tuckerman, M. E. *J. Chem. Phys.* **2007**, *126*, 164501.

(51) Lin, I.-C.; Seitsonen, A. P.; Tavernelli, I.; Rothlisberger, U. *J. Chem. Theory Comput.* **2012**, *8*, 3902−3910.

(52) Lyubartsev, A. P.; Laasonen, K.; Laaksonen, A. *J. Chem. Phys.* **2001**, *114*, 3120−3126.

(53) Heuft, J. M.; Meijer, E. J. *J. Chem. Phys.* **2003**, *119*, 11788−11791.

(54) Raugei, S.; Klein, M. L. *J. Chem. Phys.* **2002**, *116*, 196−202.

(55) Heuft, J. M.; Meijer, E. J. *J. Chem. Phys.* **2005**, *123*, 094506.

(56) White, J. A.; Schwegler, E.; Galli, G.; Gygi, F. *J. Chem. Phys.* **2000**, *113*, 4668−4673.

(57) Baerends, E. J.; Ziegler, T.; Autschbach, J.; Bashford, D.; Bérces, A.; Bickelhaupt, F. M.; Bo, C.; Boerrigter, P. M.; Cavallo, L.; Chong, D. P.; Deng, L.; Dickson, R. M.; Ellis, D. E.; van Faassen, M.; Fan, L.; Fischer, T. H.; Fonseca Guerra, C.; Ghysels, A.; Giammona, A.; van Gisbergen, S. J. A.; Götz, A. W.; Groeneveld, J. A.; Gritsenko, O. V.; Grüning, M.; Gusarov, S.; Harris, F. E.; van den Hoek, P.; Jacob, C. R.; Jacobsen, H.; Jensen, L.; Kaminski, J. W.; van Kessel, G.; Kootstra, F.; Kovalenko, A.; Krykunov, M. V.; van Lenthe, E.; McCormack, D. A.; Michalak, A.; Mitoraj, M.; Neugebauer, J.; Nicu, V. P.; Noodleman, L.; Osinga, V. P.; Patchkovskii, S.; Philipsen, P. H. T.; Post, D.; Pye, C. C.; Ravenek, W.; Rodríguez, J. I.; Ros, P.; Schipper, P. R. T.; Schreckenbach, G.; Seldenthuis, J. S.; Seth, M.; Snijders, J. G.; Solà, M.; Swart, M.; Swerhone, D.; te Velde, G.; Vernooijs, P.; Versluis, L.; Visscher, L.; Visser, O.; Wang, F.; Wesolowski, T. A.; van Wezenbeek, E. M.; Wiesenekker, G.; Wolff, S. K.; Woo, T. K.; Yakovlev, A. L. *"Amsterdam Density Functional"*, Scientific Computing and Modeling, 2012 Developer's Version. URL: http://www.scm.com (accessed July 2013).

(58) te Velde, G.; Bickelhaupt, F. M.; Baerends, E. J.; Fonseca Guerra, C.; van Gisbergen, S. J. A.; Snijders, J. G.; Ziegler, T. *J. Comput. Chem.* **2001**, *22*, 931−967.

(59) Fonseca Guerra, C.; Snijders, J. G.; te Velde, G.; Baerends, E. J. *Theor. Chem. Acc.* **1998**, *99*, 391−403.

(60) van Lenthe, E.; Baerends, E. J.; Snijders, J. G. *J. Chem. Phys.* **1993**, *99*, 4597−4610.

(61) Zhang, Y.; Yang, W. *Phys. Rev. Lett.* **1998**, *80*, 890−890.

(62) Adamo, C.; Barone, V. *J. Chem. Phys.* **1999**, *110*, 6158−6170.

(63) Schwerdtfeger, P.; Pernpointner, M.; Nazarewicz, W. Calculation of Nuclear Quadrupole Coupling Constants. In *Calculation of NMR and EPR Parameters. Theory and Applications*; Kaupp, M., Bühl, M., Malkin, V. G., Eds.; Wiley−VCH: Weinheim, Germany, 2004; pp 279−291.

(64) van Lenthe, E.; Baerends, E. J. *J. Chem. Phys.* **2000**, *112*, 8279−8292.

(65) Berendsen, H. J. C.; Postma, J. P. M.; Van Gunsteren, W. F.; Hermans, J. *Intermol. Forces* **1981**, *11*, 331−342.

(66) Odelius, M.; Laaksonen, A. Combined MD simulation-NMR relaxation studies of molecular motion and intermolecular interactions. In *Theoretical and Computational Chemistry*, Vol. 7; Balbuena, P. B., Seminario, J. M., Eds.; Elsevier: Amsterdam, 1999; pp 281−324.

(67) Advertisement by Bruker Instruments, Inc. *Anal. Chem.* **1976**, *48*, 1198A.

(68) Schmidt, P. C.; Sen, K. D.; Das, T. P.; Weiss, A. *Phys. Rev. B* **1980**, *22*, 4167−4179.

4086

dx.doi.org/10.1021/ct400419s | *J. Chem. Theory Comput.* 2013, 9, 4074−4086